

# The comparison of design airflow rates with dynamic and steady-state displacement models in varied dynamic conditions

Natalia Lastovets<sup>1</sup> (✉), Risto Kosonen<sup>1,2</sup>, Juha Jokisalo<sup>1</sup>

1. Aalto University, Department of Mechanical Engineering, Espoo, Finland

2. College of Urban Construction, Nanjing Tech University, Nanjing, China

## Abstract

A temperature-based method is usually applied in displacement ventilation (DV) design when overheating is the primary indoor climate concern. Different steady-state models have been developed and implemented to calculate airflow rate in rooms with DV. However, in practical applications, the performance of DV depends on potentially dynamic parameters, such as strength, type and location of heat gains and changing heat gain schedule. In addition, thermal mass affects dynamically changing room air temperature. The selected steady-state and dynamic models were validated with the experimental results of a lecture room and an orchestra rehearsal room. Among the presented models, dynamic DV model demonstrated a capability to take into account the combination of dynamic parameters in typical applications of DV. The design airflow rate is calculated for the case studies of dynamic DV design in the modelled lecture room in both dynamic and steady-state conditions. In dynamic conditions of heavy construction in 2–4 hours occupancy periods, the actual airflow rate required could be 50% lower than the airflow rate calculated with the steady-state models. The difference between steady-state and dynamic multi-nodal model is most significant with heavyweight construction and short occupancy period (17%–28%). In cases with light construction, the dynamic DV model provides roughly the same airflow rates for four-hour occupancy period than the Mund's model calculates. The dynamic model can significantly decrease the design airflow rate of DV, which can result in a reduction of investment costs and electrical consumption of fans.

## 1 Introduction

Displacement ventilation (DV) has been first applied in industrial buildings and since the 1980s in non-industrial applications. The basic principle of displacement ventilation is that the cool air is supplied into the occupied zone of the room at low velocity and then rises upwards from the heat sources by the vertical convection currents. As a result, room air with DV has both stratified and mixed zone with different temperature profiles. The design of displacement ventilation is usually based on controlling the desired air temperature in the occupied zone. Thus, the estimation of the vertical temperature gradient is essential in displacement ventilation design.

Design DV models with different level of complexity

E-mail: natalia.lastovets@aalto.fi

## Keywords

displacement ventilation design, airflow rate, temperature gradient, dynamic model, simplified building energy models

## Article History

Received: 24 May 2020

Revised: 26 August 2020

Accepted: 16 September 2020

© The Author(s) 2020

have been introduced in the literature. Computational fluid dynamics (CFD) provides a spatial temperature and velocity distribution by solving the airflow governing equations. Recently CFD has been successfully applied to the room airflow studies providing the most accurate and detailed results among the room air models (Nielsen 2015). However, these models are often too complicated for practical engineering calculations. Besides, CFD requires specific knowledge of this technology (Gilani et al. 2016). Coarse-grid zonal models are a compromising approach between CFD and simple nodal models. In zonal models, the room air volume is divided into several air zones with perfectly mixed air and uniform temperature (Song et al. 2008). Based on the heat and mass balance in macroscopic control volumes, they need shorter computing time but require predefined flow direction

and exchange rates of airflow between the zones (Megri and Haghighat 2007). In displacement ventilation studies, these models have been integrated with plume theory (Rees and Haves 2001) and heat gain division between the zones (Zhang et al. 2019).

The temperature gradient in DV systems is usually calculated with the nodal approach, which is suitable for design and system sizing since it provides a rapid solution (Källblad 1998). Nodal models apply the electrical analogy to represent a heat balance of the room air as an idealised network of nodes connected with airflow paths. Unlike zonal models, nodal models do not predict mass transfer in a room, so that prior knowledge of the airflow patterns is needed in order to specify mass flow in the thermal network (Griffith 2002). Until recently design guidelines from various researchers for displacement ventilation have applied two-nodal models (Li et al. 1992; Mundt 1995; Arens 2000) that predict the linear slope between the air nodes above the floor and exhaust terminal, which is assumed to be always at the ceiling. The temperature above the floor normalised between the supply and exhaust temperatures can be estimated from experimental data (Sandberg and Blomqvist 1989) or based on a simple model of the ceiling to floor heat transfer as a function of airflow rate (Mundt 1995).

Other design guidelines assume a constant vertical air temperature gradient between the head and feet ( $2^{\circ}\text{C}/\text{m}$ ) from the temperature above the floor (Skistad 1994). Since only the heat entering the occupied zone needs to be considered in displacement ventilation systems, later studies proposed fractional coefficient methods to calculate the reduced heat gains in the occupied zone (Yuan et al. 1999; Bauman 2003; Xu et al. 2009; Cheng et al. 2012; Liang et al. 2018; Zhang et al. 2018, 2019). In these methods, total room space heat gains are artificially divided into occupied and unoccupied fractions. The part of the heat gains in the occupied zone is calculated from the total heat gains with fraction coefficients. These coefficients are estimated empirically or derived from statistical methods based on a database of CFD simulation cases (Lau and Niu 2003).

The multi-nodal models introduce a temperature profile composed by variable slopes between the nodes. The models with a different number of nodes, heat gain configuration and mixing height consideration can be found in the literature (Nielsen 2003; Mateus and da Graça 2015; Lastovets et al. 2020a). These models calculate mixing height with plume theory depending on types and number of convective heat sources (Hunt and Van den Bremer 2011). The multi-nodal models provide a promising method for the temperature gradient prediction (Kosonen et al. 2016).

However, all models mentioned above have been developed for steady conditions. At the same time, air stratification created by plumes depends on potentially

dynamic parameters, such as strength, type and location of heat gains, ventilation airflow rate and supply air temperature. Besides, since DV is usually applied in non-residential buildings that are not occupied continuously, the thermal mass effect, varied internal and solar heat gains significantly reflect the room air temperatures (Ferdyn-Grygierek and Baranowski 2011; Csáky and Kalmár 2015; Coşkun et al. 2017). It means that in practical applications, the current steady-state models cannot accurately predict the room air temperature gradient in dynamic conditions. Thus, an accurate calculation of the vertical temperature gradient in dynamic conditions is required for DV design.

Building simulation programmes provide detail information about building dynamics (Harish and Kumar 2016; Wang and Zhai 2016). These programmes usually assume full-mixed room air and use empirical correlation to estimate convective and radiant heat transfer between room air and enclosure surfaces. However, these assumptions are not satisfactory for non-uniform indoor environments and spaces with flows different from that used in the fully-mixed conditions. The beneficial option can be co-simulation of detailed room air models and computer simulation that provides boundary conditions for room air models, such as room surface temperatures and heat transfer through the building envelope (Zhai and Chen 2003; Djunaedy et al. 2005). Co-simulation with CFD and zonal models is usually used for research purposes rather than engineering design due to the computation load and technological complexities (Griffith and Chen 2004; Tian et al. 2018).

Nodal models implemented in building energy simulation software is an accessible option for design. Some of the two- and multi-nodal models are applied in DV design and available in thermal energy simulation tools. The most frequently used Mundt's model (Mundt 1995) is implemented in IDA ICE (Shalin 2003) and EnergyPlus (Crawley et al. 2004). The multi-nodal DV model implemented in EnergyPlus (Mateus and da Graça 2015), together with the calculation methods of mixing height were validated in dynamic conditions with the measurements in classrooms (Mateus et al. 2016) and large rooms (Mateus and da Graça 2017). The principle of heat gain breakdown applied in the Mateus model (Mateus et al. 2016) was later developed in the multi-nodal DV model and validated for different heat gain types and combinations of them (Lastovets et al. 2020a). While the assumption of unified air temperature over the mixing height has been applied in the previously developed multi-nodal models, the model used in the current study (Lastovets et al. 2020b) allows accounting for both type and vertical position of the indoor heat gains.

Simplified building energy models are still practical for pre-design and system sizing in typical applications due to their user-friendliness and straightforward calculation

(Kramer et al. 2012). Among the simplified models, the most common are the resistance–capacitance (RC) models of a building zone that imply thermal–electrical analogy based on the similarity between electric current and heat flux. In this approach, an RC-network of a building zone represents every element of the building construction elements and room air with heat capacities and conductances (Parnis 2012).

Since displacement ventilation is usually designed in the spaces that are not continuously occupied, the thermal mass effect and occupancy schedules significantly reflect the room air temperatures. Occupancy schedules are often analysed for energy simulation (Ahmed et al. 2017) building control systems (Oldewurtel et al. 2013) and data-driven models of occupant behaviour (Piselli and Pisello 2019). However, the influence of occupancy schedules on the design airflow rate with DV has not been studied in detail.

The thermal mass effect on indoor air temperature change has been analysed in many pieces of research. The RC models of building constructions allow studying the effect of external and internal thermal mass on indoor air temperature for different configurations, including lightweight and heavyweight structures (Zhou et al. 2008). The thermal mass effect of different constructions is especially noticeable with night ventilation (Solgi et al. 2018). Artman (2009) studied the influence of heat gains, airflow rates, building construction and climatic conditions on the dynamic change of room air temperatures with night ventilation. Besides, the temperature difference between indoor and outdoor air temperature during night was found as a crucial factor of night ventilation performance. The effect of window orientation on indoor air temperatures has been studied experimentally for the ideally mixed air conditions (Givoni and Hoffman 1966; Csáky and Kalmár 2015). The detailed studies were conducted for hot climates (Al-Tamimi et al. 2011; Bekkouche et al. 2013). However, the effect of thermal mass and building orientation is usually studied under full-mixed air conditions. Thus, there is a lack of experimental and numerical studies dedicated to the effect of the combination of thermal mass with different constructions and night ventilation and window orientation to the room temperature gradient with DV.

The present study applies a simplified dynamic DV model to calculate the vertical temperature gradient (Lastovets et al. 2020b) that integrates the multi-nodal DV model (Lastovets et al. 2020a) and two-capacity building energy model (UNI EN 2008; Sirén 2016). The heat capacities and conductances of the dynamic multi-nodal model are calibrated against the results taken from the dynamic building simulation model IDA ICE (Shalin 1996) and validated in a lecture room and an orchestra rehearsal room. The validated dynamic is further used in a case room analysis, where the

design airflow rates of the steady-state and dynamic models are compared. The paper studies the difference of the selected state-state and dynamic displacement models in dynamic conditions, where the effect of different heat load breakdowns, occupancy periods and thermal mass levels on design airflow rate is analysed. The novelty of this research comes from the use of the model in displacement ventilation design and validation of the presented method with the measurements. The paper gives an insight into the investment savings potential when dynamic displacement model is introduced.

## 2 Methods

This section introduces the methods to evaluate the feasibility of different models in displacement ventilation (DV) design. This section presents steady-state and dynamic design models of DV. The models are first validated with measurements for two typical applications in a lecture hall and an orchestra rehearsal room. To get a general view of the meaning of different parameters, the effect of thermal mass, heat gain breakdowns and time schedules on the design airflow rate is analysed in a case room with steady-state and dynamic models.

### 2.1 Design models of DV

The studied design DV methods represent the analytical energy balance approach with lumped parameters. These models treat the building room air as an idealised network of air temperature nodes connected with airflow convection conductances (Griffith 2002). In these nodal models, the room surface temperatures are coupled convectively to air temperatures and by long-wave radiation to each other. The transmission heat transfer through the room structures is calculated with the RC (resistance–capacitance) method (Parnis 2012).

#### 2.1.1 Steady-state design DV models

Two steady-state nodal models with different numbers of nodes and heat gain configuration were chosen for the present analysis. The Mundt model (Mundt 1995) estimates linear vertical temperature gradient over the room height ( $H$ ) between the air temperature along the floor at the height 0.1 m ( $T_{0.1}$ ) and the exhaust temperature ( $T_{ex}$ ) (Figure 1(a)).

The multi-nodal DV model (Lastovets et al. 2020a) calculates the temperature profile composed by variable slopes between the nodes (Figure 1(b)). This model calculates the height of air temperature stratification ( $h_{mx}$ ) with the vertical heat gain breakdown. The mixing height is the transition level between a mixed upper layer and stratified layer, which relates to the height where the supply airflow

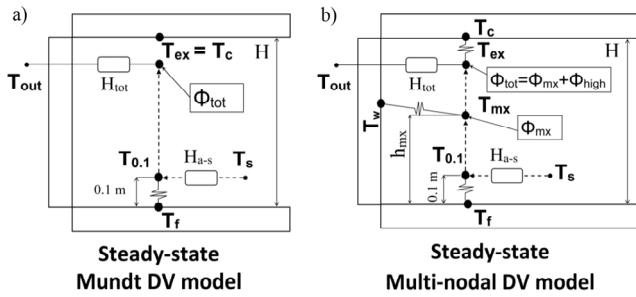


Fig. 1 Steady-state displacement ventilation design models

rate matches the airflow induced by the thermal plumes in the occupied zone.

In the Mundt model, the convective heat flux at the floor is balanced with the air temperature rise near the floor from the supply air temperature ( $T_s$ ) to air temperature at 0.1 height ( $T_{0.1}$ ):

$$H_{a-s} \cdot (T_{0.1} - T_s) = \alpha_{c,f} \cdot A_f \cdot (T_f - T_{0.1}) \quad (1)$$

where:  $H_{a-s}$  is the heat conductance of ventilation ( $W/^\circ C$ );  $\alpha_{c,f}$  is the convective heat transfer coefficient at the floor surface ( $\alpha_{c,f} = 3 W/(m^2 \cdot ^\circ C)$ );  $A_f$  is the floor area ( $m^2$ ). The heat transfer coefficients are taken from the recommendation given in the model description (Mundt 1995; Yuan et al. 1999).

The heat conductance of ventilation ( $H_{a-s}$ ) is calculated from the air properties and supply airflow rate:

$$H_{a-s} = \rho \cdot c_p \cdot q_v \quad (2)$$

where  $\rho$  is the air density ( $kg/m^3$ ),  $q_v$  is the supply airflow rate ( $m^3/s$ ) and  $c_p$  is the specific heat of the air ( $J/(kg \cdot ^\circ C)$ ).

In Mundt's model (Mundt 1995) the radiative heat transfer from the ceiling to the floor maintains the energy balance on the floor surface. The model assumes that the radiative energy flux from the floor is balanced by convective heat transfer from the floor surface to the air (Eq. (3)). This assumption works well with the measurements in the most cases but could lead to wrong temperature prediction when the radiative heat transfer to the floor is small (Yuan et al. 1999). The exhaust air temperature ( $T_{ex}$ ) is assumed to be the same than the ceiling temperature (Eq. (4)).

$$\alpha_{r,f} \cdot A_f \cdot (T_{ex} - T_f) = \alpha_{c,f} \cdot A_f \cdot (T_f - T_{0.1}) \quad (3)$$

where:  $\alpha_{r,f}$  is the radiative heat transfer coefficient at the floor surface ( $\alpha_{r,f} = 5.5 W/(m^2 \cdot ^\circ C)$ ).

The radiative heat transfer coefficient in all the models may be set to  $5.5 W/(m^2 \cdot ^\circ C)$  for a common temperature range in ventilated rooms (UNI EN 2005a).

The exhaust air temperature is calculated from the room air heat balance (Eq. (4)). In this model, the indoor air stratification is neglected. However, since the transmission heat transfer is often not significant because of a small

difference between indoor and outdoor air temperatures, this simplification is adequate in the typical applications of displacement ventilation.

$$H_{a-s} \cdot (T_{ex} - T_s) + H_{tot} \cdot (T_{ex} - T_{out}) = \Phi_{tot} \quad (4)$$

where  $\Phi_{tot}$  is the total heat gains ( $W$ );  $H_{tot}$  is the total conductance of building structures ( $W/^\circ C$ );  $T_{out}$  is the outside air temperature ( $^\circ C$ ).

The total heat conductance ( $H_{tot}$ ) determines transmission heat transfer through structures of the building envelope as follows:

$$H_{tot} = U_{tot} \cdot A_{tot} \quad (5)$$

where  $U_{tot}$  is the total  $U$ -value of the building envelope ( $W/(m^2 \cdot ^\circ C)$ ) and  $A_{tot}$  is the envelope area of the room ( $m^2$ ). The total  $U$ -value of the building envelope is calculated based on standards that were developed in the European Committee for Standardisation (CEN) and the International Organisation for Standardisation (ISO) (UNI EN 2005a).

The steady-state multi-nodal model calculates three air temperatures at the height of 0.1 m, at the height of the mixed layer ( $h_{mx}$ ) and the height of the exhaust air temperature that is equal to the room height. The mixing height is calculated with the point source model of plume theory (Kosonen et al. 2017):

$$h_{mx} = (k_q^p)^{-\frac{3}{5}} \cdot \left(\frac{q_v}{n}\right)^{\frac{3}{5}} \cdot \Phi_c^{-\frac{1}{5}} + h_0^{ver} \quad (6)$$

where:  $h_{mx}$  is the mixing height ( $m$ );  $q_v$  is a supply airflow rate ( $m^3/s$ ),  $\Phi_c$  is a convective heat gain of the vertical buoyancy source ( $W$ ),  $n$  is the number of thermal plumes,  $h_0^{ver}$  is a virtual origin height ( $m$ ),  $k_q^p$  is an entrainment coefficient for a point source plume ( $k_q^p = 0.005$ ).

The present study applies the conical correlation with the "minimum" approach (Kosonen et al. 2017) to calculate the virtual origin height above the vertical heat source:

$$h_0^{ver} = H_s - 1.47 \cdot D \quad (7)$$

where  $H_s$  is the height of the heat source (1.1 m) and  $D$  is the diameter of the heat source (0.4 m). The height and diameter of the vertical heat source correspond to the size of the cylindrical human body simulator (DIN 4715-1 1995) that produce similar buoyancy flux to the realistic body shape (Zukowska et al. 2007).

Heat gain distribution determines the convection heat transfer connection between the wall surfaces and air nodes. The model consists of the set of three convection and three radiation heat balance equations assuming 50% split between the convective and radiative heat gains. The energy conservation equations for the three model air temperatures



determined. In the calibration, mixing ventilation is used, and thus, the air temperature  $T_a$  is the same than the exhaust air temperature. The calibration method consists of two phases where steady-state and dynamic set response parameters are separately calibrated. During the steady-state calibration, IDA-ICE tool controlled the heating power of the room to reach the constant room air temperature setpoint 21 °C. The division of this conductance to  $H_{m-out}$  and  $H_{a-m}$  and two capacities  $C_a$  and  $C_m$  are determined in the dynamic parameter identification by applying a step response method through a sudden change in heating power.

The dynamic DV model represents six first-order differential equations to calculate three air and three mass temperatures for the vertical temperature profile:

$$C_a \frac{dT_{ex}}{dt} = H_{a-out} (T_{out} - T_{ex}) + H_{a-m} (T_c - T_{ex}) + H_{a-s} (T_s - T_{ex}) + \Phi_{tot} \quad (15)$$

$$C_m \frac{dT_c}{dt} = H_{m-s} (T_{out} - T_c) + H_{a-m} (T_{ex} - T_c) + \alpha_{r,c} A_{tot} \left( \frac{T_w A_w + T_f A_f}{A_{tot} - A_c} - T_c \right) \quad (16)$$

$$C_a \frac{dT_{mx}}{dt} = H_{a-out} (T_{out} - T_{mx}) + H_{a-m} (T_w - T_{mx}) + H_{a-s} (T_s - T_{mx}) + \Phi_{mx} \quad (17)$$

$$C_m \frac{dT_w}{dt} = H_{m-s} (T_{out} - T_w) + H_{a-m} (T_{mx} - T_w) + \alpha_{r,w} A_{tot} \left( \frac{T_c A_c + T_f A_f}{A_{tot} - A_w} - T_w \right) \quad (18)$$

$$C_a \frac{dT_{0.1}}{dt} = H_{a-out} (T_{out} - T_{0.1}) + H_{a-m} (T_f - T_{0.1}) + H_{a-s} (T_s - T_{0.1}) \quad (19)$$

$$C_m \frac{dT_f}{dt} = H_{m-s} (T_{out} - T_f) + H_{a-m} (T_{0.1} - T_f) + \alpha_{r,f} A_{tot} \left( \frac{T_c A_c + T_w A_w}{A_{tot} - A_f} - T_f \right) \quad (20)$$

The differential equations can be solved numerically with the Euler method since there is no tendency for numerical oscillations (Sirén 2016).

## 2.2 Measurements for validation of design DV models

The measurements for two typical applications of DV in the lecture hall (Lastovets et al. 2020b) and orchestra rehearsal room (Mateus and da Graça 2017) are selected for the validation of dynamic DV model. These spaces differ from each other in different ceiling height, thermal mass, heat load breakdowns and time schedules.

### 2.2.1 Lecture hall

The lecture hall (Lastovets et al. 2020b) with the floor area 108 m<sup>2</sup> is located at Aalto University (Espoo, Finland). The room does not have any outdoor walls since it is located in the central part of the second floor of the building. The air is supplied through 50 diffusers located under the seats and extracted from five exhaust grilles. The exhaust grilles are located near the ceiling height (3 m) along the corridor walls (Figure 3).

For measuring air temperatures at different heights from floor to ceiling, the measuring mast was assembled with 20 TinyTag loggers (Gemini Data Loggers 2018) (accuracy ±0.4 °C). Seventeen TinyTags were located at ten centimetres distance, starting from 0.1 m to 1.7 m, followed by three more loggers at 2 m, 2.5 m and 3 m, respectively. Swema 200 md manometer was used for measuring airflow rates from individual diffusers (±0.3 of reading, accuracy ±0.3 Pa).

The lecture hall construction includes internal glazing and remaining heavy concrete opaque surfaces. The internal thermal mass takes into account the furniture in the studied room. The IDA ICE model of a lecture hall was created to calibrate the conductances and capacitances of the two-capacity model. The wall structures were modelled according to the design values. For simplicity, rectangular geometry was used in the IDA ICE model. The floor area was adjusted according to the volume of the studied room. The internal staircase was also shrimped to equal floor thickness and added to the floor area (Table 1).

### 2.2.2 Orchestra rehearsal room

The Orchestra rehearsal room (Mateus and da Graça 2017) with the area 325 m<sup>2</sup> and 7 m height has a maximum capacity for 150 musicians. The air is supplied through wall perforated low-velocity units hidden by architectural wood panels and extracted at the ceiling level. Eight temperature sensors on a vertical mast measure the room air temperatures

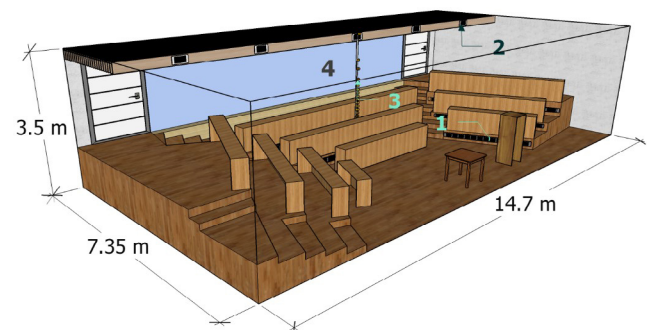


**Fig. 3** The layout of the lecture room and the location of the measurement (notations: 1 – DV diffusers; 2 – exhaust air grilles; 3 – location of the air temperature measurements; 4 – internal glazing)

**Table 1** Constructions of the lecture hall

Room surfaces	Area (m <sup>2</sup> )	Construction	Thickness (m)	Thermal conductivity (W/(m·K))	Density (kg/m <sup>3</sup> )	Specific heat (J/(kg·K))	U-value (W/(m <sup>2</sup> ·K))
Floor	86.4	Floor covering	0.005	0.18	1100	920	2.90
		Concrete	0.250	1.70	2300	880	
Internal staircase	20.1	Wood layer	0.020	0.14	500	2300	1.29
		Air	0.200	0.53	1.2	1006	
		Concrete	0.150	1.70	2300	880	
Ceiling	86.4	Wood	0.100	0.14	500	2300	0.17
		Concrete	0.150	1.70	2300	880	
Walls	87.9	Render	0.020	0.80	1800	790	0.53
		Lightweight concrete	0.250	0.15	500	1050	
Doors	5.9	Wood	0.040	0.14	500	2300	2.19
Glazing	23.8						1.90
Internal mass	53.8	Furniture	0.027	0.13	1000	1300	2.50

(Figure 4). The room air temperature was measured with the Luft weather station (accuracy  $\pm 0.2$  °C) (Mateus and da Graça 2017). The room constructions consist of heavyweight (ceiling) and light (floor, walls) concrete. The area of the furniture is taken into account by adding internal masses of 60 m<sup>2</sup> furniture (Table 2).

### 2.3 Case study room

The effect of thermal mass, heat gain breakdowns and time schedules on the design airflow rate are analysed in a case room with steady-state and dynamic models. The case room is a typical lecture room with the floor area 100 m<sup>2</sup> and window area 15 m<sup>2</sup> (Figure 5).

Two types of building constructions, heavyweight concrete (Table 3) and lightweight timber frame (Table 4) are analysed in the case studies, while *U*-values of all the types of constructions are kept the same. The window glazing *U*-value was 1.9 W/(m<sup>2</sup>·°C).

The effect of the heat gain breakdown on the design airflow rate is studied with different combinations of heat gains where the ration of occupants, lighting and solar

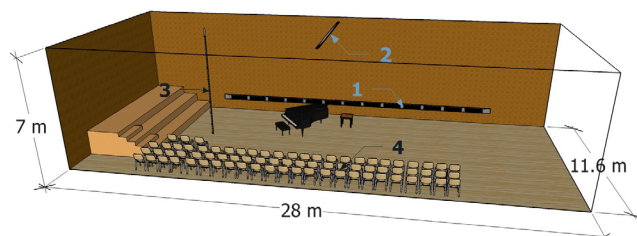


**Fig. 4** The layout of the orchestra rehearsal room and the location of the measurement (notations: 1 – DV diffusers; 2 – exhaust air grilles; 3 – location of the air temperature measurements; 4 – occupancy area)

radiation were varied. The total heat gain was constant 6 kW in all the cases (Table 5).

In all the cases, the operation schedule of fans with the design airflow rate was as follows:

- night ventilation by using cold outdoor air with start-stop optimisation of fans between 0:00 and 08:00,
- normal operation mode with mechanical cooling between 08:00 and 18:00 and
- the fans were off between 18:00 and 24:00.

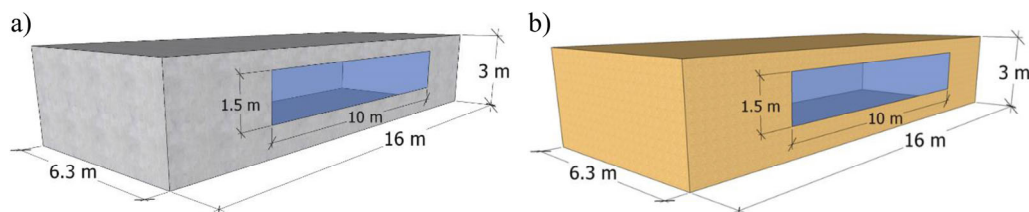
During the regular operation hours, the supply air temperature for mechanical cooling was constant at 19 °C. The supply air temperature was assumed to be the same as the outdoor temperature during the night ventilation. The start-stop optimisation of the night ventilation controlled the running time of fans to provide the room air temperature 22 °C ( $\pm 0.1$  °C) at 8 a.m. It practically means that night ventilation was used either continuously between 0:00 and 08:00 or night ventilation was introduced for some hours in early hours before the occupancy period, depending on the case.

The room air temperature in the occupied zone locates at the height 1.1 m, that represents the room air temperature at the neck level of a seating person (UNI EN 2005b). The air temperature at this height is typically applied as a design air temperature in a room with seated people. The steady-state design models calculate the design airflow rate to provide the target occupied zone temperature of 25 °C. The design airflow rate in the dynamic DV model was iterated to fulfil the set of the maximum target room air temperature (25 °C) during the occupied hours and also early morning temperature at 8 a.m. (22 °C) before the occupied hours. In the dynamic design method used, the airflow rate iterated was always constant during the night and day

**Table 2** Constructions of the orchestra rehearsal room

Room surfaces	Area (m <sup>2</sup> )	Material	Thickness (m)	Thermal conductivity (W/(m·K))	Density (kg/m <sup>3</sup> )	Specific heat (J/(kg·K))	U-value (W/(m <sup>2</sup> ·K))
Lightweight concrete wall	554	Concrete	0.30	0.27	750	1000	0.78
Concrete ceiling	325	Insulation	0.02	0.04	N/A (20*)	N/A (750*)	1.14
		Concrete	0.30	2.00	2100	880	
Lightweight concrete floor	325	Concrete	0.30	0.27	750	1000	0.78
Internal masses	60*	Furniture	0.03	0.13	1000	1300	2.50

\*Estimated values

**Fig. 5** The modelled lecture room with concrete (a) and timber frame (b) constructions**Table 3** Heavyweight constructions

	Material	Thickness (m)	Thermal conductivity (W/(m·K))	Density (kg/m <sup>3</sup> )	Specific heat (J/(kg·K))	U-value (W/(m <sup>2</sup> ·K))
Concrete wall	Concrete	0.250	1.700	2300	880	0.22
	Light insulation	0.150	0.036	20	750	
Concrete ceiling	Light insulation	0.150	0.036	20	750	0.22
	Concrete	0.250	1.700	2300	880	
Concrete floor	Floor coating	0.005	0.18	1100	920	0.22
	Light insulation	0.150	0.036	20	750	
	Concrete	0.250	1.700	2300	880	

**Table 4** Lightweight constructions

	Material	Thickness (m)	Thermal conductivity (W/(m·K))	Density (kg/m <sup>3</sup> )	Specific heat (J/(kg·K))	U-value (W/(m <sup>2</sup> ·K))
Timber frame wall	Gypsum	0.026	0.220	970	1090	0.23
	Frames and min. wool	0.195	0.052	92	2010	
	Gypsum	0.009	0.220	970	1090	
	Wood	0.025	0.140	500	2300	
L/W Ceiling	Insulation	0.150	0.036	20	750	0.22
	Wood	0.022	0.140	500	2300	
	Gypsum	0.013	0.220	970	1090	
L/W concrete floor	Floor coating	0.005	0.180	1100	920	0.22
	Insulation	0.100	0.036	20	750	
	L/W concrete	0.250	0.150	500	1050	

time operation hours.

The weather conditions of the design day were chosen from the Finnish test reference year (Kalamees et al. 2012) (Figure 6). The hourly heat gain of the solar radiation was

calculated using the scaling coefficients from the maximum value for the west (Figure 7(a)) and east oriented façades (Figure 7(b)). For the steady-state models, the mean average outside temperature is applied.

**Table 5** Case studies in the model lecture room

		Cases															
		Heavyweight constructions															
		1a	1b	1c	1d	1e	1f	1g	1h	1i	1j	1k	1l	1m	1n	1o	1p
		8 h profile (9–17)						4 h profile (2h 9–11 and 2h 15–17)						2 h (09–11)		2 h (15–17)	
		Lightweight constructions															
2a	2b	2c	2d	2e	2f	2g	2h	2i	2j	2k	2l	2m	2n	2o	2p		
8 h profile (9–17)						4 h profile (2h 9–11 and 2h 15–17)						2 h (09–11)		2 h (15–17)			
Window orientation		s	w	s	w	—	—	s	w	s	w	—	—	s	s	w	w
6 kW heat gains breakdown (kW)	Occupants	3	3	4	4	5	6	3	3	4	4	5	6	3	4	3	4
	Lighting	1	1	—	—	1	—	1	1	—	—	1	—	1	—	1	—
	Max solar heat gains	2	2	2	2	—	—	2	2	2	2	—	—	2	2	2	2

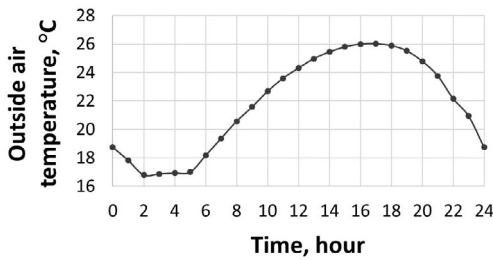


**Fig. 6** Outdoor air temperatures of the design day

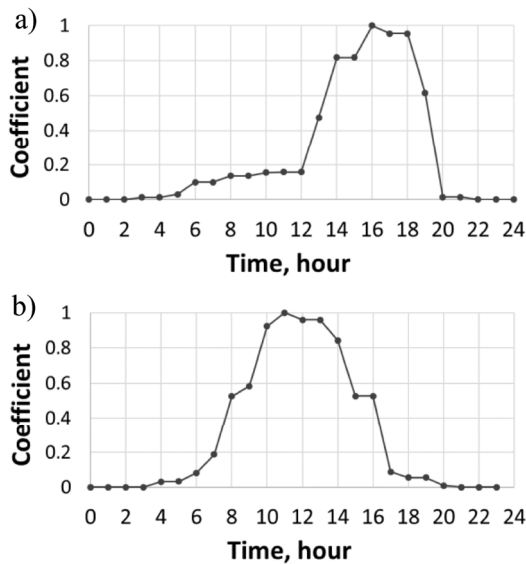


**Fig. 7** Hourly profile of the solar heat gains on the west (a) and south (b) oriented façades

### 3 Results

#### 3.1 Validation of the design DV models

This section presents the validation of the DV design models (Figures 1 and 2) with measurements in the lecture hall (Figure 3) and the orchestra rehearsal room (Figure 4) to

estimate the capability of the DV models to calculate the occupied zone temperature. The simulation models of both validation spaces were modelled in the building simulation software IDA ICE to calibrate the heat capacities  $C_a$  and  $C_m$  and conductances  $H_{m-out}$  and  $H_{a-m}$  of the dynamic multi-nodal DV model. The calibration method is presented in detail in Lastovets et al. (2020b) publication. The calibration is conducted for fully-mixed conditions, and thus, the air temperature is the same as the exhaust air temperature. The calibration method consists of two phases where steady-state and dynamic set response parameters are separately calibrated. In the calibration, the total conductance  $H_{tot}$  is defined in the steady-state parameter identification. The division of this conductance to  $H_{m-out}$  and  $H_{a-m}$  and two capacities  $C_a$  and  $C_m$  are determined in the dynamic parameter identification.

In the studied cases, the internal heat gains, supply air temperatures, outdoor air temperatures and airflow rates were constant. The total heat gains in both validation cases consisted of the heat gains from occupants and lighting.

##### 3.1.1 Validation of the design DV models in the lecture hall

The lecture hall had heavyweight concrete building structures and relatively high internal thermal mass (Table 1). The duration of the validation was 1 hour and 50 minutes in the lecture hall. The heat gains of sitting people were estimated to be 100 W per person, and the lighting heat gains were 2.5 kW. The measurements were carried out between on the 28th of October 2017 in a lecture room at Aalto University (Espoo, Finland). The air temperature of neighbouring rooms was 21 °C provided by the heating system in winter conditions. Since the room does not have any outdoor walls, the cooling demand is caused by the internal heat gains from the occupants and lighting. Table 6 presents the validation case of the lecture hall.

Table 7 presents the calibrated total conductance  $H_{tot}$

**Table 6** The description of the validation cases in the lecture hall

Number of people	Internal heat gains (W)			Outside air temperature (°C)	Supply air temperature (°C)	Airflow rate (m <sup>3</sup> /s)
	Occupants (60 W/m <sup>2</sup> )	Lighting (23 W/m <sup>2</sup> )	Total (83 W/m <sup>2</sup> )			
65	6500	2500	9000	21	18	0.6

**Table 7** The calibrated parameters of the dynamic DV model in the lecture hall

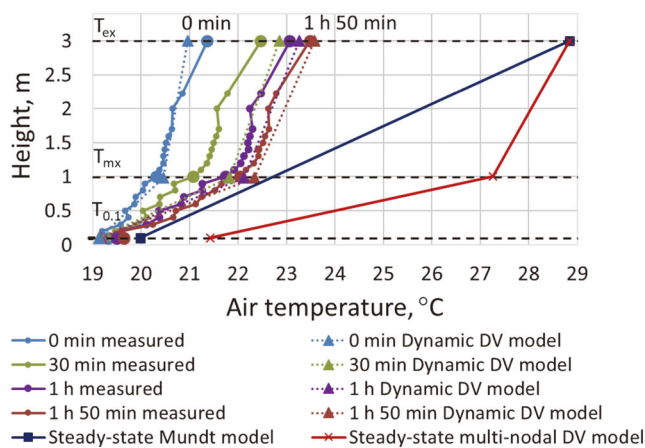
$H_{tot}$ (W/K)	$H_{a-m}$ (W/K)	$H_{m-out}$ (W/K)	$C_a$ (kJ/K)	$C_m$ (kJ/K)
102	1431	110	1636	48701

conductances  $H_{am}$  and  $H_{ms}$  and heat capacities  $C_a$  and  $C_m$  of the multi-nodal DV model for the lecture hall.

Figure 8 shows the measured and simulated vertical temperature gradients during the validation period. The heights of the temperatures modelled at  $T_{0.1}$ ,  $T_{mx}$  and  $T_{ex}$  are marked with dotted lines. The temperature profiles in a lecture hall show the typical vertical temperature distribution with a displacement ventilation system. With the supply air temperature lower than the room air temperature, the convection flow of sitting students displaced upwards the air supplied. As a result, the vertical temperature gradients with well-defined mixing height were developed. The heat gains from ceiling-mounted lamps caused the temperature gradient above the mixing height.

The thermal mass of heavyweight structures had an essential role in the development of the room air temperature, and during 1 h 50 mins test period the temperature was not yet reached the steady-state condition. It should be noted that the profile of the room air temperature was quite similar during the test period when the temperature continuously raised up to the mixing height (around 1 m level).

Even though the multi-nodal model is more accurate than the linearised Mundt's model in steady-state conditions

**Fig. 8** Vertical air temperature gradients measured and calculated with the dynamic and steady-state design DV models in the lecture hall

(Kosonen et al. 2016), in dynamic conditions, both models overestimate the predicted temperature gradient in rooms with DV. It reveals the importance to take into account the dynamic behaviour of the thermal mass in the modelling.

The temperature gradient below 1 m height calculated with the Mundt's model was closer to the measurement results than the gradient calculated with the steady-state multi-nodal model. However, the dynamic multi-nodal model provided an accurate prediction of the evolution of the vertical air temperature profile at all heights ( $T_{ex}$ ;  $T_{mx}$  and  $T_{0.1}$ ). Also, the room air temperature modelling as a function of time was close to the measured values.

### 3.1.2 Validation of the design DV models in the orchestra rehearsal room

The orchestra rehearsal room had a higher ceiling and a bigger floor area than the lecture hall. Most of the building structures consisted of lightweight concrete (Table 2). The measurements in the orchestra rehearsal room were performed for 1 hour 20 minutes with 65 occupants and specific heat gains of 120 W per practising person. The room had relatively high heat gains from lighting (21 W/m<sup>2</sup>). The outside air temperature was 18 °C during the measurements. Table 8 presents the validation case of the orchestra rehearsal room.

Table 9 presents the calibrated total conductance  $H_{tot}$ , conductances  $H_{am}$  and  $H_{ms}$  and heat capacities  $C_a$  and  $C_m$  of the multi-nodal DV model for the orchestra rehearsal room.

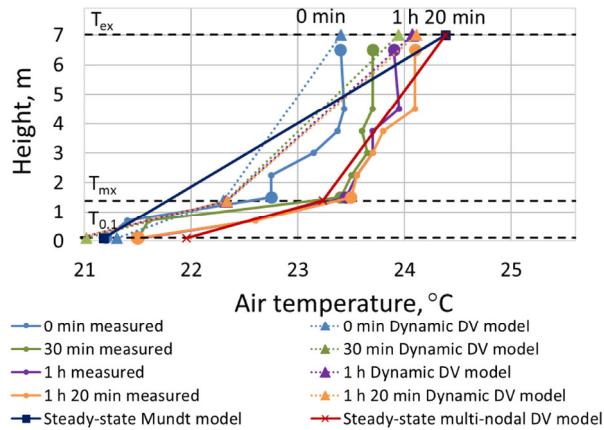
Figure 9 shows the measured and simulated vertical temperature gradients during the validation period, and the heights of the temperatures modelled at  $T_{0.1}$ ,  $T_{mx}$  and  $T_{ex}$  are marked with dotted lines in Figure 9. As in the lecture hall case, the vertical temperature stratification profiles measured in the orchestra rehearsal room (Figure 9) depicted two distinct regions below and upper the mixing height. However, the air temperatures stabilised quickly (in 30 minutes) at the occupant level of the orchestra rehearsal room. It can happen due to comparatively low difference (about 1 °C) between the temperatures of supply air and room air in the occupied zone combined with high specific

**Table 8** The description of the validation cases in the orchestra rehearsal room

Number of people	Internal heat gains (W)			Outside air temperature (°C)	Supply air temperature (°C)	Airflow rate (m <sup>3</sup> /s)
	Occupants (24 W/m <sup>2</sup> )	Lighting (21 W/m <sup>2</sup> )	Total (45 W/m <sup>2</sup> )			
65	7800	9200	17000	18	21	2.8

**Table 9** The calibrated parameters of the dynamic DV model in the orchestra rehearsal room

$H_{tot}$ (W/K)	$H_{a-m}$ (W/K)	$H_{m-out}$ (W/K)	$C_a$ (kJ/K)	$C_m$ (kJ/K)
857	4154	1080	4010	87017

**Fig. 9** Vertical air temperature gradients measured and calculated with the dynamic and steady-state design DV models in the orchestra rehearsal room

airflow rate (8.6 L/(s·m<sup>2</sup>)). As a result, the convective effect of the human thermal plume is getting weaker, which causes air mixing between the near-floor layer and space above (Espinosa and Glicksman 2017). As a result, the air temperatures are quickly getting closer to the steady-state values (Figure 7).

In the lecture hall with the supply air temperature, 2.3°C lower than the room air temperature and specific airflow rate (5.6 L/(s·m<sup>2</sup>)) one third lower than in the orchestra rehearsal room, the thermal plumes of the sitting students caused slower growth of the vertical room temperatures (Figure 8).

The effect of different ventilation design configurations on the temperature profile of the air in rooms with DV is convenient to represent by Archimedes number ( $Ar$ ), which compares the effects of buoyancy and supply momentum (Nielsen 2003). The Archimedes number in the occupied zone at the height 1.1 m ( $Ar_{1.1}$ ) can be presented as follows:

$$Ar_{1.1} = \frac{g \cdot \beta \cdot h_{1.1} \cdot (T_{1.1} - T_s)}{\left(\frac{q_v}{A_f}\right)^2} \quad (21)$$

where  $\beta$  is the thermal expansion coefficient (°C<sup>-1</sup>),  $g$  is the acceleration of gravity (m/s<sup>2</sup>),  $h_{1.1}$  is the room height 1.1 m,

$T_{1.1}$  is the air temperature at the height 1.1 m (°C);  $T_s$  is the supply air temperature (°C),  $q_v$  is the airflow rate to the room (m<sup>3</sup>/s),  $A_f$  is the floor area of the room (m<sup>2</sup>).

The high Archimedes number in the lecture hall case ( $Ar = 40 \cdot 10^3$ ) at the beginning of the measurements indicates the dominant phenomenon of the buoyancy of convective flow induced by the human thermal plume. In this case, the dynamic DV design model is capable of predicting the vertical temperature gradient.

The five times lower  $Ar$  number in the orchestra rehearsal room ( $Ar = 8 \cdot 10^3$ ) points out the weaker convective effect of thermal plumes from occupants, which affects the typical air temperature distribution assumed by the dynamic DV model. That reveals the limitation of the dynamic DV model for the cases with low initial air temperature differences and/or high-momentum flows ( $Ar < 10 \cdot 10^3$ ). It could also cause different heat gain of lighting estimated by the dynamic DV model (Lastovets et al. 2020a).

In this case, the dynamic multi-nodal DV model underpredicted the dynamic behaviour of the occupied zone temperature. The temperature in the occupied zone was roughly 0.5–1 °C higher than the measured values. Mundt's model underpredicted the stabilised air temperatures in the occupied zone by more than 1–1.5 °C.

### 3.2 Case studies

This section presents the calculation of the design airflow rate by the DV models (Figures 1 and 2) in the modelled case study lecture room (100 m<sup>2</sup>) (Figure 5) with heavy and lightweight constructions (Tables 3 and 4), window orientations (west and south), heat gain breakdowns and occupancy schedules. Table 10 presents the calibrated total conductance  $H_{tot}$ , conductances  $H_{am}$  and  $H_{ms}$  and heat capacities  $C_a$  and  $C_m$  of the multi-nodal DV model for the modelled case study lecture room.

In the case study analysis, the total heat load of 6 kW was fixed to be constant in all the cases, but the combinations of heat gains breakdown in occupied and upper zones varied. During the occupied hours, the heat gains from lighting and persons were constant during the occupied periods,

and the heat gains from solar radiation varied depending on the window orientation (Figure 7). The required airflow rates were calculated for three occupancy profiles: 8 hours continuous usage (09:00–17:00), two separate two-hour periods during the day (09:00–11:00 and 15:00–17:00) and 2 hours continuous usage (09:00–11:00 or 15:00–17:00). With the cases of two- and four-hour usages, the design conditions occurred at the same time when the maximum solar radiation occurred. The effect of different window orientations, occupied periods and heat gain breakdowns on the design airflow rate was analysed for both heavy (Table 11) and lightweight (Table 12) constructions.

Since Mundt's model does not take into account the usage profile and thermal mass, it led the same airflow rate of 0.4 m<sup>3</sup>/s in all the cases analysed with 6 kW heat gain. The steady-state multi-nodal DV model takes into account the heat gain breakdown when the airflow rate is determined. When all 6 kW heat gains occurred in the occupied zone, the required design airflow rate was 0.76 m<sup>3</sup>/s, whereas,

with the upper-level lighting heat gain of 1 kW, it was 0.69 m<sup>3</sup>/s (Table 11). Thus, the linear Mundt's model provided 42%–47% lower design airflow rate than the more detailed steady-state multi-nodal model. However, it should be emphasised that the Mundt's model underestimates the airflow rate required in steady-state conditions, and the target room air temperature cannot be achieved at the occupied zone. In those steady-state conditions, the multi-nodal model is more accurate than Mundt's model (Kosonen et al. 2016).

In addition to taking into account the heat gain breakdown, the dynamic multi-nodal DV model provided different values of airflow rates depending on building thermal mass, changing heat gains and occupied periods. The dynamic multi-nodal DV model calculated the lowest airflow rate with massive constructions. In the case with high thermal mass, it is possible to utilise night ventilation efficiently. Therefore, the calculated airflow rate was lower than with the state-state models. The required airflow

**Table 10** The calibrated parameters of the dynamic DV model in the modelled case study lecture room

Construction	$H_{tot}$ (W/K)	$H_{a,m}$ (W/K)	$H_{m,out}$ (W/K)	$H_{a,out}$ (W/K)	$C_a$ (kJ/K)	$C_m$ (kJ/K)
Heavyweight	70	1543	73	29	1464	60440
Lightweight	70	1319	73	29	1496	13210

**Table 11** Design airflow rates of three different calculation models for heavy construction

Case	Window orientation	8 h profile (9–17)					
		6 kW heat gains breakdown (occupied/upper zone) (kW)			Airflow rate with different DV design models (m <sup>3</sup> /s)		
		Occupants	Lighting	Max solar heat gains	Mundt steady-state model	Multi-nodal steady-state model	Multi-nodal dynamic model
1a	South	3	1	2	0.40	0.69	0.33
1b	West	3	1	2	0.40	0.69	0.30
1c	South	4	N/A	2	0.40	0.76	0.35
1d	West	4	N/A	2	0.40	0.76	0.38
1e	N/A	5	1	N/A	0.40	0.69	0.33
1f	N/A	6	N/A	N/A	0.40	0.76	0.43
4 h profile (2 h 9–11 and 2 h 15–17)							
1g	South	3	1	2	0.40	0.69	0.24
1h	West	3	1	2	0.40	0.69	0.21
1i	South	4	N/A	2	0.40	0.76	0.26
1j	West	4	N/A	2	0.40	0.76	0.29
1k	N/A	5	1	N/A	0.40	0.69	0.20
1l	N/A	6	N/A	N/A	0.40	0.76	0.31
2 h profile (09–11)							
1m	South	3	1	2	0.40	0.69	0.19
1n	South	4	N/A	2	0.40	0.76	0.20
2 h profile (15–17)							
1o	West	3	1	2	0.40	0.69	0.16
1p	West	4	N/A	2	0.40	0.76	0.23

**Table 12** Design airflow rates of three different calculation models for lightweight construction

Case	Window orientation	8 h profile (9–17)					
		6 kW heat gains breakdown (occupied/upper zone) (kW)			Airflow rate with different DV design models (m <sup>3</sup> /s)		
		Occupants	Lighting	Max solar heat gains	Mundt model steady-state	Multi-nodal steady-state model	Multi-nodal dynamic model
2a	South	3	1	2	0.40	0.69	0.39
2b	West	3	1	2	0.40	0.69	0.44
2c	South	4	N/A	2	0.40	0.76	0.51
2d	West	4	N/A	2	0.40	0.76	0.58
2e	—	5	1	N/A	0.40	0.69	0.53
2f	—	6	N/A	N/A	0.40	0.76	0.63
4 h profile (2 h 9–11 and 2 h 15–17)							
2g	South	3	1	2	0.40	0.69	0.26
2h	West	3	1	2	0.40	0.69	0.35
2i	South	4	N/A	2	0.40	0.76	0.38
2j	West	4	N/A	2	0.40	0.76	0.45
2k	N/A	5	1	N/A	0.40	0.69	0.35
2l	N/A	6	N/A	N/A	0.40	0.76	0.44
2 h profile (09–11)							
2m	South	3	1	2	0.40	0.69	0.25
2n	South	4	N/A	2	0.40	0.76	0.37
2 h profile (15–17)							
2o	West	3	1	2	0.40	0.69	0.29
2p	West	4	N/A	2	0.40	0.76	0.41

rate is 0.19–0.38 m<sup>3</sup>/s, which is 24%–5% lower than with Mundt's model and 36%–49% lower than the steady-state multi-nodal model calculated (Table 11). It indicates that the thermal mass and dynamic usage profile are playing a significant role in the determination of the design airflow rate. Only in the case of 8 hours continuous occupancy with persons only, the airflow rate calculated with the dynamic DV model is slightly higher than with steady-state Mundt's model. The reason for the higher airflow rate is high concentrated heat gains in the occupied zone that requires more supply air to maintain the set target temperature. It has been noted in the previous studies (Kosonen et al. 2016), that the room air temperature is constant in the upper zone when the major part of heat gains is located in the occupied zone. In this kind of cases, the linear vertical temperature gradient between the floor and ceiling is not developed, and the maximum benefits of displacement ventilation are not reached (Kosonen et al. 2016).

Shortening of the occupancy period with the heavy structure led to a significant reduction in the design airflow rate for all the studied cases (Table 10). The reduction of the continuously occupied period from 8 hours to 4 hours resulted in 28% decrease in the required airflow rate. When the occupied period was reduced from 8 hours to 2 hours,

the airflow rate decreased by more than 50%. It is quite significant reduction in the spaces, e.g. theatres or concert halls where the steady model could overestimate the requirement of the airflow rate.

The orientation of the window affected the calculated airflow rate differently. In the morning hours, the heat gains from solar radiation were higher on the south-facing façade than on the west-facing façade. However, the heat gains on the west-facing façade were growing faster during the occupied periods (Figure 7). In the cases with the heavyweight construction and the lowest ratio of heat gains in the occupied zone, the estimated airflow rate with south-oriented windows was 0.03 m<sup>3</sup>/s (9%–15%) higher than with west-oriented windows. In all other cases with west-oriented windows, the design airflow rate was 0.03 m<sup>3</sup>/s higher because of the fast growth of heat gains from solar radiation during the occupied hours.

The lightweight construction reacts faster to temperature changes than the heavyweight construction, and the required airflow rates increased compared with the heavy construction (Table 12). The utilisation of thermal mass with night ventilation was not efficient with the lightweight construction. Hence, the design airflow rates of the light construction with the same heat gain (breakdown and usage

profile) were 49%–16% higher than with the heavyweight construction.

The calculated airflow rates in the cases of heat gains located in the upper zone (lighting) were on the average 0.12 m<sup>3</sup>/s (27%) lower than in the cases where all heat gains are located in the occupied zone (persons only). Also, the orientation of the window effects on the design airflow rate. The airflow rates in the cases with south-oriented windows were on the average 12% lower than the values calculated with west-oriented windows (Table 12).

With light construction, the reduction of the occupancy period from continuous 8 hours to 4 hours resulted in a 20%–33% decrease in the airflow rate (Table 12). However, the difference in airflow rates between the cases with four- and

two-hour occupancy periods was just 0.01 m<sup>3</sup>/s–0.04 m<sup>3</sup>/s (4%–9%). It indicates that with light construction and short occupancy periods, the thermal mass is playing a significant role.

It should be noted that in some cases, Mundt’s steady-model air flow rate is lower than the one predicted by the multi-nodal dynamic model. Especially in the cases where the major part of the heat gains is in the occupied zone, the dynamic model gives higher airflow rates than Mundt’s model. In most of the cases with 4 hours of 2 hours occupancy, the design airflow rate of the dynamic multi-nodal model is lower than with Mundt’s model.

Figures 10 and 11 present the room air temperatures of west and south oriented rooms during the design day with

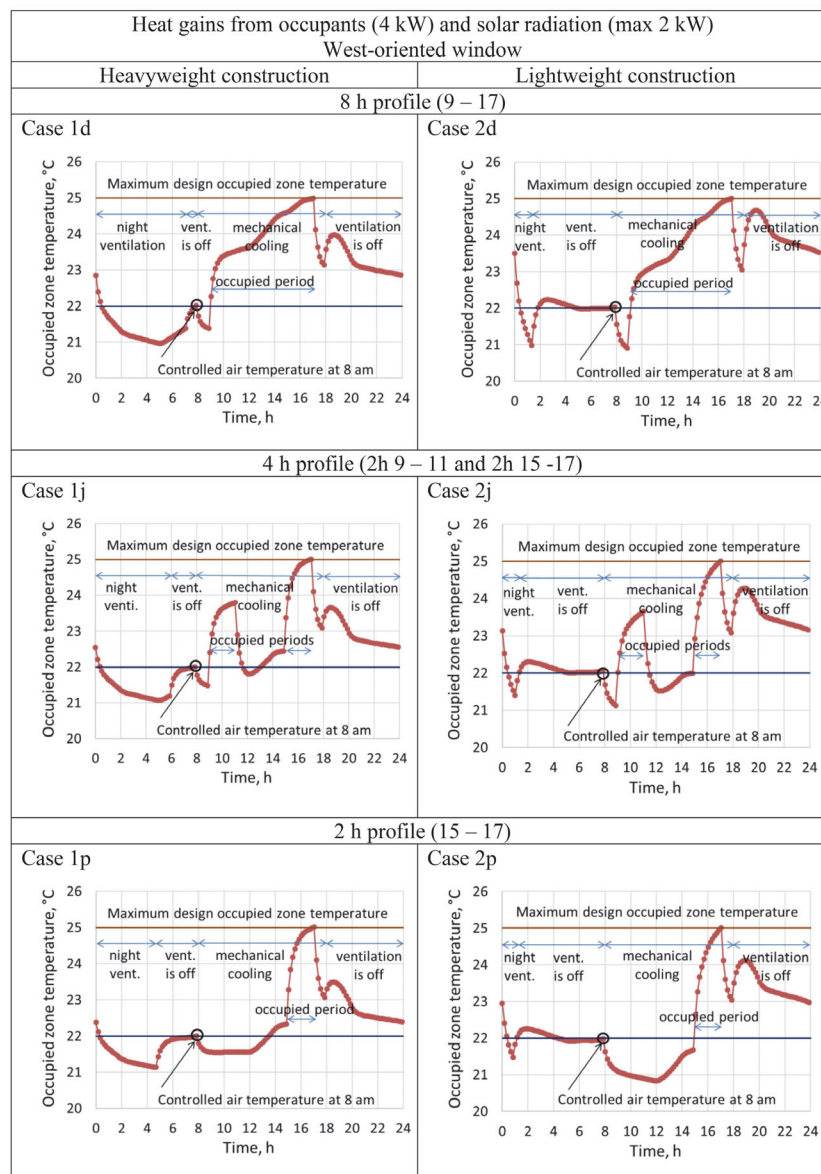


Fig. 10 Room air temperatures at the occupied zone with the dynamic DV multi-nodal model using different heat gain profiles in the west-oriented room

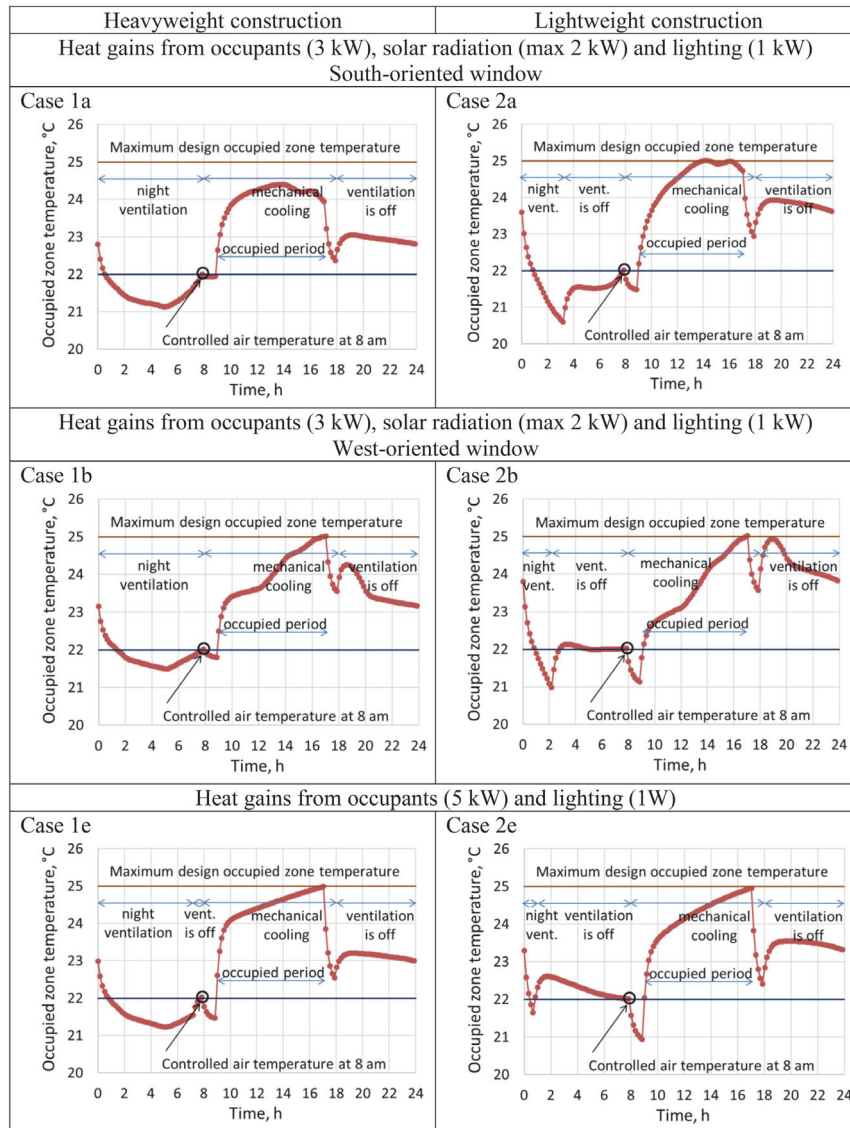


Fig. 11 Room air temperatures at the occupied zone with the dynamic DV multi-nodal model using different heat gain breakdowns

the dynamic multi-nodal model for the cases with heavy and lightweight constructions. In Figure 10, the effect of the occupancy hours is presented, and the effect of the heat gain breakdown is presented in Figure 11, respectively.

The results showed that the lightweight construction reacts much faster to the night ventilation than heavy constructions for the same heat gain profile (Figure 10). The running hours of night ventilation indicate the effect of thermal mass in energy storage that reduced the actual cooling load in the operation hours. With the heavyweight construction, night-time ventilation is used from 2 to 5 hours depending on the case, while with the lightweight construction it is only required around 1-hour time to reduce the room air temperature to 22 °C required at 8 a.m.

Figure 11 presents the dynamic changes in air temperature in the occupied zone in the cases with different breakdowns

of heat gains in the occupied zone. In the cases of the solar heat gains, the time of maximum room air temperature occurred at the same time as the maximum solar radiation. In the cases without solar radiation, the maximum temperature was at the end of the occupancy period. In the cases of the south-oriented window (Figure 11 Cases 1a and 2a), the solar heat gains slowly grow during the occupied period, causing steady changing of the room air temperature. While with the west-oriented window (Figure 11 Cases 1b and 2b), the room air temperature changed fast when the solar heat gain is introduced after 12 p.m.

#### 4 Discussion

In the existing DV design practice, the supply airflow rate is calculated either with the heat balance method or air

quality-based methods (Kosonen et al. 2017). The air quality-based design by applying thermal plume theory is used only in industrial types of applications where high contaminant loads exist. In non-industrial premises, e.g. in theatres, design practice is based on the minimum airflow rate per person of local building codes (e.g. 6 L/s) (Kavgic et al. 2008). Heat balance is the most common method in DV design. Heat balance method is applied in rooms where room air temperature in the occupied zone is the primary design criterion. In this case, the airflow rate is usually calculated with steady-state models. In some cases, the steady-state heat balance method overestimates the design airflow rate (Lastovets et al. 2020a).

Many studies investigated the effect of thermal mass on room air temperature with night ventilation (Yang and Li 2008). They demonstrated the ability of night ventilation to improve comfort conditions and reduce cooling load (Blondeau et al. 1997). Massive heavy constructions utilise night ventilation well in a cold climate. However, in a hot tropical climate, lightweight construction with low thermal mass is preferable (Wang et al. 2009; Roberz et al. 2017). Thus, the use of night ventilation should be examined on a case-by-case basis in the early design stages; the conditions when night ventilation and thermal mass are sufficient as a passive cooling design strategy.

Even though some building energy simulation software (e.g., EnergyPlus and IDA ICE) include the model of the thermal environment with displacement ventilation, they are limited to the specific system configuration (Citherlet et al. 2001). In addition, the utilisation of those models requires prior knowledge of both the indoor thermal environment simulation and building energy simulation, which could be a challenge to a building energy engineer.

The commonly used models to design displacement ventilation are based on steady-state temperature gradient calculation with simplified nodal models, among which the multi-nodal models are the most accurate (Kosonen et al. 2016; Lastovets et al. 2020b). However, for accurate design, these models are insufficient in the estimation of room air temperatures due to the missing effect of thermal mass and varied heat loads during operation time. Steady-state approach and neglecting the dynamic behaviour of heat loads and thermal mass could lead to significant overestimation of the required airflow rate. Thus, the dynamic approach is appreciated in the DV system design.

The presented dynamic DV model predicts the dynamic behaviour of the thermal mass and room air vertical temperature gradient with a good level of accuracy. However, this model has certain limitations. Since all internal mass, such as floors, walls and furniture, are presented in the model as one entity, it is not able to take into account different thermal properties of individual structures. On

the other hand, it could be assumed that in a typical application, it would not significantly affect the thermal behaviour. The dynamic DV model is able to predict within reasonable accuracy the thermal behaviour of typical buildings where the only relatively small active thickness of the structure interacts with the regularly varied heat gains (Johannesson 1981; Ghoreishi and Ali 2011).

In steady-state conditions, Mundt's linearised model underestimates occupied zone air temperature by up to 3 °C and provides unrealistic vertical air temperature profile (Kosonen et al. 2016). However, in the cases with significant lighting heat loads and short occupied period, Mundt's model calculates airflow rate close to the dynamic DV model.

The vertical heat gain breakdown significantly affects temperature stratification. Some recommendations of how to divide the heat gains between different vertical zones in rooms with thermally stratified environments are available in the scientific literature (Schiavon et al. 2011; Cheng et al. 2012). Nevertheless, the complexity of transient air flows in rooms with ununiform vertical temperature distribution could cause uncertainty in temperature gradient calculations with simplified lumped-parameter models.

Since the premises with DV are usually not occupied continuously, the dynamic model of room air vertical temperature gradient is appreciated in DV design. The possible application of the presented dynamic DV model is in the rooms where different dynamic factors, such as heat gain variation, location and type of heat gains and building thermal mass have a different effect on indoor thermal conditions. Typical applications are in concert halls that are occupied for a short time and in lobbies that are influenced by highly varied internal heat loads and solar radiation.

## 5 Conclusion

The estimation of the vertical temperature gradient reflects airflow rate calculation and thermal comfort estimation in rooms with displacement ventilation (DV). At the moment, it is common to use a steady-state model that do not take occupancy profiles and thermal mass into account. In this study, two steady-state and one dynamic DV model were validated with measurements in terms of accuracy and dynamics of room air temperature changes in different vertical levels in two typical applications. Besides, the design airflow rate was calculated with different models in both dynamic and steady-state conditions in a modelled case study room. In the cases analysed, the airflow rate calculated with the dynamic DV model is significantly lower than the airflow rate calculated with the steady-state DV models. The difference between steady-state and dynamic multi-nodal models is most significant with heavyweight construction

and short occupancy period. Hence, considering dynamic conditions in 2–4 hours occupancy periods, the actual airflow rate could be 50% lower than the airflow rate calculated with the steady-state models.

Shortening of the occupancy periods from eight- to four-hour results in roughly three times lower required airflow rate with both heavy and lightweight constructions. The difference between the steady-state and dynamic multi-nodal models is most significant with heavyweight construction and short occupancy period. Thus, the reduction of the occupancy periods from four- to two-hour in the cases with heavyweight construction leads to 17%–28% lower airflow rate. In contrast, with lightweight construction, the decrease of airflow rate due to the same reduction of the occupied hours is only 4%–9%. The design airflow rate calculated with the dynamic DV model is lower than the values estimated by Mundt's model for all occupancy periods with heavyweight construction. Nevertheless, the airflow rates calculated with the dynamic model and lightweight construction were 28% higher than the values given by Mundt model for eight-hour occupancy period and roughly the same for four-hour usage profile.

The time of maximum heat gains determines the maximum design occupied zone temperature. Thus, the orientation of the windows differently affected the calculated airflow rate. In most cases with west-oriented windows, the design airflow rate was on average 11% higher than in a south-oriented room.

The dynamic model can significantly decrease the design airflow rate of DV, which can result in a reduction of investment costs and electrical consumption of fans. The presented calibrated multi-nodal dynamic DV model is able to take into account varied heat loads and the effect of building thermal mass within good accuracy. The dynamic DV model can be applied in DV design with various applications where heat gains varied, and thermal mass is playing a significant role. The model has good robustness to predict thermal performance under different operation conditions.

### Acknowledgements

The authors are grateful for the funding provided by the School of Engineering of Aalto University. Special thanks to Aalto University Properties (ACRE) and Fidelix Oy for the assistance with the measurements and the arrangement of the measurement setup.

**Funding note:** Open access funding provided by Aalto University.

**Open Access:** This article is licensed under a Creative Commons Attribution 4.0 International License, which permits use, sharing, adaptation, distribution and reproduction in any medium or format, as long as you give appropriate credit to the original author(s) and the source, provide a link to the Creative Commons licence, and indicate if changes were made.

The images or other third party material in this article are included in the article's Creative Commons licence, unless indicated otherwise in a credit line to the material. If material is not included in the article's Creative Commons licence and your intended use is not permitted by statutory regulation or exceeds the permitted use, you will need to obtain permission directly from the copyright holder.

To view a copy of this licence, visit <http://creativecommons.org/licenses/by/4.0/>

### References

- Ahmed K, Akhondzada A, Kurnitski J, Olesen B (2017). Occupancy schedules for energy simulation in new prEN16798-1 and ISO/FDIS 17772-1 standards. *Sustainable Cities and Society*, 35: 134–144.
- Al-Tamimi NAM, Fadzil SFS, Harun WMW (2011). The effects of orientation, ventilation, and varied WWR on the thermal performance of residential rooms in the tropics. *Journal of Sustainable Development*, 4: 142–149.
- Arens AD (2000). Evaluation of displacement ventilation for use in high-ceiling facilities. Master Thesis, Massachusetts Institute of Technology, USA.
- Artmann N (2009). Cooling of the building structure by night-time ventilation. PhD Thesis, Aalborg University, Denmark.
- Bauman FS (2003). Underfloor Air Distribution (UFAD) Design Guide. Atlanta: American Society of Heating, Refrigerating and Air-Conditioning Engineers.
- Bekkouche SMEA, Benouaz T, Cherier MK, Hamdani M, Yaiche MR, et al. (2013). Influence of building orientation on internal temperature in Saharan climates, building located in Ghardaïa region (Algeria). *Thermal Science*, 17: 349–364.
- Blondeau P, Spérandio M, Allard F (1997). Night ventilation for building cooling in summer. *Solar Energy*, 61: 327–335.
- Cheng Y, Niu J, Gao N (2012). Stratified air distribution systems in a large lecture theatre: A numerical method to optimize thermal comfort and maximize energy saving. *Energy and Buildings*, 55: 515–525.
- Citherlet S, Clarke JA, Hand J (2001). Integration in building physics simulation. *Energy and Buildings*, 33: 451–461.
- Coşkun T, Turhan C, Arsan ZD, Akkurt GG (2017). The importance of internal heat gains for building cooling design. *Journal of Thermal Engineering*, 3: 1060–1064
- Crawley DB, Lawrie LK, Pedersen CO, Winkelmann FC (2004). EnergyPlus: An update. In: Proceedings of SimBuild 2004, Building Sustainability and Performance Through Simulation, Boulder, CO, USA.

- Csáky I, Kalmár F (2015). Effects of thermal mass, ventilation, and glazing orientation on indoor air temperature in buildings. *Journal of Building Physics*, 39: 189–204.
- da Graça GCC (2003). Simplified models for heat transfer in rooms. PhD Thesis, University of California, San Diego, USA.
- Davies MG (1984). An approximate expression for room view factors. *Building and Environment*, 19: 217–219.
- Davies MG (1990). Room heat needs in relation to comfort temperature: Simplified calculation methods. *Building Services Engineering Research and Technology*, 11: 129–139.
- DIN 4715-1 (1995). Chilled Surfaces for Rooms. Part 1. Measuring of the Performance with Free Flow—Test Rules (English version), Deutsche Institut für Normung.
- Djunaedy E, Hensen JLM, Loomans MGLC (2005). External coupling between CFD and energy simulation: implementation and validation. *ASHRAE Transactions*, 111(1): 612–624.
- Espinosa FD, Glicksman LR (2017). Determining thermal stratification in rooms with high supply momentum. *Building and Environment*, 112: 99–114.
- Ferdyn-Grygierek J, Baranowski A (2011). Energy demand in the office buildings for various internal heat gains. *Architecture Civil engineering Environment*, 4: 89–93.
- Gemini Data Loggers (2018) Tinytag Plus 2 Dual Channel Temperature/Relative Humidity (–25 to +85°C/0 to 100% RH) TGP-4500. Issue 12: 2nd March 2018 (E&OE). <http://gemini2.assets.d3r.com/pdfs/original/3242-tgp-4500.pdf>. Accessed 23 May 2020.
- Ghoreishi AH, Ali MM (2011). Contribution of thermal mass to energy performance of buildings: A comparative analysis. *International Journal of Sustainable Building Technology and Urban Development*, 2: 245–252.
- Gilani S, Montazeri H, Blocken B (2016). CFD simulation of stratified indoor environment in displacement ventilation: Validation and sensitivity analysis. *Building and Environment*, 95: 299–313.
- Givoni B, Hoffman E (1966). Effect of window orientation on indoor air temperature. *Architectural Science Review*, 9: 80–83.
- Griffith BT (2002). Incorporating nodal and zonal room air models into building energy calculation procedures. Master Thesis, Massachusetts Institute of Technology, USA.
- Griffith B, Chen QY (2004). Framework for coupling room air models to heat balance model load and energy calculations (RP-1222). *HVAC&R Research*, 10: 91–111.
- Harish VSKV, Kumar A (2016). A review on modeling and simulation of building energy systems. *Renewable and Sustainable Energy Reviews*, 56: 1272–1292.
- Hunt GR, Van den Bremer TS (2011). Classical plume theory: 1937–2010 and beyond. *IMA Journal of Applied Mathematics*, 76: 424–448.
- Johannesson G (1981). Active heat capacity: Models and parameters for the thermal performance of buildings, PhD Thesis, Lund Institute of Technology, Sweden.
- Kalamees T, Jylhä K, Tietäväinen H, Jokisalo J, Ilomets S, et al. (2012). Development of weighting factors for climate variables for selecting the energy reference year according to the EN ISO 15927-4 standard. *Energy and Buildings*, 47: 53–60.
- Källblad K (1998). Thermal models of buildings. Determination of temperatures, heating and cooling loads. Theories, models and computer programs. Report TABK–98/1015, Building Science, Lund Technical University, Sweden.
- Kavgic M, Mumovic D, Stevanovic Z, Young A (2008). Analysis of thermal comfort and indoor air quality in a mechanically ventilated theatre. *Energy and Buildings*, 40: 1334–1343.
- Kosonen R, Lastovets N, Mustakallio P, da Graça GC, Mateus NM, et al. (2016). The effect of typical buoyant flow elements and heat load combinations on room air temperature profile with displacement ventilation. *Building and Environment*, 108: 207–219.
- Kosonen R, Melikov A, Mundt E, Mustakallio P, Nielsen PV (2017). Displacement Ventilation, REHVA Guidebook No 23. Forssa: Federation of European Heating and Air-Conditioning Associations.
- Kramer R, Van Schijndel J, Schellen H (2012). Simplified thermal and hygric building models: A literature review. *Frontiers of Architectural Research*, 1: 318–325.
- Lastovets N, Kosonen R, Mustakallio P, Jokisalo J, Li A (2020a). Modelling of room air temperature profile with displacement ventilation. *International Journal of Ventilation*, 19: 112–126.
- Lastovets N, Sirén K, Kosonen R, Jokisalo J, Kilpeläinen S (2020b). Dynamic performance of displacement ventilation in a lecture hall. *International Journal of Ventilation*, 1: 1–11.
- Lau J, Niu JL (2003). Measurement and CFD simulation of the temperature stratification in an atrium using a floor level air supply method. *Indoor and Built Environment*, 12: 265–280.
- Li Y, Sandberg M, Fuchs L (1992). Vertical temperature profiles in rooms ventilated by displacement: Full-scale measurement and nodal modelling. *Indoor Air*, 2: 225–243.
- Liang C, Shao X, Melikov AK, Li X (2018). Cooling load for the design of air terminals in a general non-uniform indoor environment oriented to local requirements. *Energy and Buildings*, 174: 603–618.
- Mateus NM, da Graça GC (2015). A validated three-node model for displacement ventilation. *Building and Environment*, 84: 50–59.
- Mateus NM, Simões GN, Lúcio C, da Graça GC (2016). Comparison of measured and simulated performance of natural displacement ventilation systems for classrooms. *Energy and Buildings*, 133: 185–196.
- Mateus NM, da Graça GC (2017). Simulated and measured performance of displacement ventilation systems in large rooms. *Building and Environment*, 114: 470–482.
- Megri AC, Haghghat F (2007). Zonal modeling for simulating indoor environment of buildings: Review, recent developments, and applications. *HVAC&R Research*, 13: 887–905.
- Mundt E (1995). Displacement ventilation systems—Convection flows and temperature gradients. *Building and Environment*, 30: 129–133.
- Nielsen PV (2003). Temperature and air velocity distribution in rooms ventilated by displacement ventilation. In: Proceedings of the 7th International Symposium on Ventilation for Contaminant Control (Ventilation 2003), Sapporo, Japan.
- Nielsen PV (2015). Fifty years of CFD for room air distribution. *Building and Environment*, 91: 78–90.
- Novoselac A, Burley BJ, Srebric J (2006). Development of new and validation of existing convection correlations for rooms with displacement ventilation systems. *Energy and Buildings*, 38: 163–173.

- Oldewurtel F, Sturzenegger D, Morari M (2013). Importance of occupancy information for building climate control. *Applied Energy*, 101: 521–532.
- Parnis G (2012). Building thermal modelling using electric circuit simulation. PhD Thesis, University of New South Wales, Australia.
- Piselli C, Pisello AL (2019). Occupant behavior long-term continuous monitoring integrated to prediction models: Impact on office building energy performance. *Energy*, 176: 667–681.
- Rees SJ, Haves P (2001). A nodal model for displacement ventilation and chilled ceiling systems in office spaces. *Building and Environment*, 36: 753–762.
- Robetz F, Loonen RCGM, Hoes P, Hensen JLM (2017). Ultra-lightweight concrete: Energy and comfort performance evaluation in relation to buildings with low and high thermal mass. *Energy and Buildings*, 138: 432–442.
- Sandberg M, Blomqvist C (1989). Displacement ventilation systems in office rooms. *ASHRAE Transactions*, 95(2): 1041–1049.
- Schiavon S, Lee KH, Bauman F, Webster T (2011). Simplified calculation method for design cooling loads in underfloor air distribution (UFAD) systems. *Energy and Buildings*, 43: 517–528.
- Shalin P (1996). Modelling and simulation methods for modular continuous system in buildings. PhD Thesis, Royal Institute of Technology (KTH), Sweden.
- Shalin P (2003). On the effects of decoupling air flow and heat balance in building simulation models. *ASHRAE Transactions*, 109(2): 788–800.
- Sirén K (2016). Course material: A simple model for the dynamic computation of building heating and cooling demand, Aalto University, Finland. [https://mycourses.aalto.fi/pluginfile.php/317972/mod\\_resource/content/1/Building%20energy%20calculation\\_Sep\\_2016.pdf](https://mycourses.aalto.fi/pluginfile.php/317972/mod_resource/content/1/Building%20energy%20calculation_Sep_2016.pdf). Assessed 23 May 2020.
- Skistad H (1994). Displacement Ventilation. Somerset, UK: Research Studies Press.
- Solgi E, Hamedani Z, Fernando R, Skates H, Orji NE (2018). A literature review of night ventilation strategies in buildings. *Energy and Buildings*, 173: 337–352.
- Song F, Zhao B, Yang X, Jiang Y, Gopal V, et al. (2008). A new approach on zonal modeling of indoor environment with mechanical ventilation. *Building and Environment*, 43: 278–286.
- Tian W, Han X, Zuo W, Sohn MD (2018). Building energy simulation coupled with CFD for indoor environment: A critical review and recent applications. *Energy and Buildings*, 165: 184–199.
- UNI EN (2005a). ISO 13792:2005. Thermal Performance of Buildings. Calculation of Internal Temperatures of a Room in Summer Without Mechanical Cooling. Simplified Methods. Geneva: International Organization for Standardization.
- UNI EN (2005b). ISO 7730:2005. Ergonomics of the Thermal Environment—Analytical Determination and Interpretation of Thermal Comfort Using Calculation of the PMV and PPD Indices and Local Thermal Comfort Criteria. Geneva: International Organization for Standardization.
- UNI EN (2008). ISO 13790: 2008. Energy Performance of Buildings—Calculation of Energy Use for Space Heating and Cooling. Geneva: International Organization for Standardization.
- Wang Z, Yi L, Gao F (2009). Night ventilation control strategies in office buildings. *Solar Energy*, 83: 1902–1913.
- Wang H, Zhai ZJ (2016). Advances in building simulation and computational techniques: A review between 1987 and 2014. *Energy and Buildings*, 128: 319–335.
- Xu H, Gao N, Niu J (2009). A method to generate effective cooling load factors for stratified air distribution systems using a floor-level air supply. *HVAC&R Research*, 15: 915–930.
- Yang L, Li Y (2008). Cooling load reduction by using thermal mass and night ventilation. *Energy and Buildings*, 40: 2052–2058.
- Yuan X, Chen Q, Glicksman LR (1999). Models for prediction of temperature difference and ventilation effectiveness with displacement ventilation. *ASHRAE Transactions*, 105(1): 353–367.
- Zhai Z, Chen QY (2003). Solution characters of iterative coupling between energy simulation and CFD programs. *Energy and Buildings*, 35: 493–505.
- Zhang S, Cheng Y, Huan C, Lin Z (2018). Heat removal efficiency based multi-node model for both stratum ventilation and displacement ventilation. *Building and Environment*, 143: 24–35.
- Zhang S, Cheng Y, Huan C, Lin Z (2019). Equivalent room air temperature based cooling load estimation method for stratum ventilation and displacement ventilation. *Building and Environment*, 148: 67–81.
- Zhou J, Zhang G, Lin Y, Li Y (2008). Coupling of thermal mass and natural ventilation in buildings. *Energy and Buildings*, 40: 979–986.
- Zukowska D, Melikov A, Popiolek Z (2007). Thermal plume above a simulated sitting person with different complexity of body geometry. In: Proceedings of the 10th International Conference on Air Distribution in Rooms (Roomvent), Kongens Lyngby, Denmark.